Chemical and magnetic interactions in Mn- and Fe-codoped Ge diluted magnetic semiconductors

Amitesh Paul*
Helmholtz-Zentrum Berlin für Materialien und Energie GmbH, Structural Research Division Methods and Instruments, Glienicker Straße 100, D-14109 Berlin, Germany

Biplab Sanyal
Department of Physics and Materials Science, Uppsala University, Box 530, SE-75121 Uppsala, Sweden
(Received 13 May 2009; published 30 June 2009)

Chemical and magnetic homogeneities of Mn and Fe, codoped in Ge, have been studied experimentally and theoretically. As we alter the codopant concentration in our diluted magnetic semiconductors, polarized neutron reflectivity measurements indicate no segregation and lower clustering tendencies for higher Fe doping. First-principles density-functional calculations based on Korringa-Kohn-Rostoker coherent-potential approximation show that Fe codoping introduces ferromagnetic interaction between Fe atoms as well as between Fe and Mn in contrast to only Mn-doped Ge. The clustering behavior observed in Mn-doped Ge is counteracted by the presence of Fe and hence increases the fraction of homogeneity, in agreement with the experiments. These observations indicate that Fe codoping makes Mn-doped Ge more attractive toward application.

DOI: 10.1103/PhysRevB.79.214438 PACS number(s): 75.50.Pp, 71.55.Cn, 85.75.−d

I. INTRODUCTION

In recent years one of the most remarkable achievements in spintronics was the observation of hole-mediated ferromagnetism in III-V diluted magnetic semiconductors (DMSs).[1] However, the growth of group-IV ferromagnetic (FM) semiconductors such as Mn_xGe_{1-x} has also triggered strong interest in searching for higher ordering temperatures T_C in Ge-based compounds.[2] The FM behavior is attributed to the $\frac{5}{2}Mn^{2+}$ ions that are substituted for Ge. These ions, acting as acceptors, generate holes that mediate the ferromagnetic exchange interaction.

Due to the low solubility of transition-metal species there exists a strong tendency to form heterogeneous regions within the Ge matrix. Generally in pure transition-metal-doped semiconductors, a strong clustering tendency between the transition metals is observed.[3,4] In Mn-based DMS, Mn atoms are often susceptible to surface segregation or form segregated phases during annealing.[5] Such phases make the interpretation of ferromagnetic behavior ambiguous as isolated domains may be formed.[6] To avoid this, one may opt for multiple transition-metal codoping that can provide the necessary stability. Recently, it was reported[7,8] on the synthesis of such a candidate DMS: an alloy of Ge, Fe, and Mn. An addition of Fe to MnGe enables us to conserve the epitaxial growth for higher total concentrations of magnetic species, which results in an increase in T_C. Very recently, codoping with Co has also been shown to magnetically complement Mn.[9]

However, an increase in T_C with Fe codoping may also be attributed to clustering or inhomogeneous distribution of magnetic species in the Ge matrix. A series of specimens has been investigated earlier,[7,8] where doping constituents and their variations have been studied in detail. Therefore, in this paper we report on the investigation of two codoped DMS specimens, codoped with alternating but unequal concentrations of Fe and Mn. Any variation in Mn-Fe distribution (homogeneity) in the two DMS specimens (with alternate concentration of codoped magnetic species), in terms of chemical as well as magnetic composition for the entire thickness of the film, has been effectively explored by depth-sensitive polarized neutron reflectivity (PNR).[10,11] These compositions represent two extreme regimes and were particularly chosen as any intermediate composition would have been impossible to identify from the rest. Surface-sensitive technique, such as x-ray absorption spectroscopy, is particularly limited in our case. Our experimental results are strongly supported by first-principles calculations, elucidating the complex magnetic and chemical interactions in Mn and Fe codoped in Ge.

II. EXPERIMENT

Experiments have been done on two samples with different compositions: $[Ge(40\ Å)/Fe(4\ Å)/Mn(2\ Å)]_{\times 11}/ZnS(550\ Å)$ named "DMS4Fe2Mn" and $[Ge(40\ Å)/Fe(2\ Å)/Mn(4\ Å)]_{\times 11}/ZnS(550\ Å)$ named "DMS2Fe4Mn." The samples are grown by molecular beam epitaxy; the details can be found elsewhere.[8] Oxidation of top layers are prevented by the thick cap layer.[12] When the Ge thickness becomes comparable with the diffusion length of Mn and Fe in Ge, a chemically homogeneous material without interfaces is formed after postdeposition annealing (allowing redistribution of species as observed from x-ray reflectivity measurements) at $T_A = 300\ °C$.[13] Magnetization measurements by a superconducting quantum interference device (SQUID) and magnetotransport measurements revealed ferromagnetic ordering but showed two different T_C's at 205 K and above 300 K for "DMS2Fe4Mn." which we have related to two magnetic phases.[8] Interestingly, "DMS4Fe2Mn" does not show the high-T_C phase and appears in the cross-sectional transmission electron microscope (TEM) image to be fairly homogeneous compared to the other sample, which showed the formation of precipitates.[8,13,14]

We performed measurements of the specimens on a neutron reflectometer at two different sources. The instruments

are TREFF(HADAS) at FMR-2(FRJ-2).[13,15] On TREFF/HADAS polarization channels of the specular reflectivities are measured by two-dimensional position sensitive detector.[16] The measurements are done at different external fields H_a in monochromatic mode for wavelength $\lambda = 4.52$ Å on HADAS ($\lambda = 4.73$ Å on TREFF) covering a normal wave-vector transfer ($Q_\perp = \frac{2\pi}{\lambda}[\sin(\alpha_i) + \sin(\alpha_f)]$). The measurements from TREFF are done without polarization analysis. In specular geometry the angle of incidence α_i equals the final angle α_f, and λ from the band is selected by a monochromator. All measurements are done after the sample was cooled to 50 and 250 K from RT by a continuous flow cryostat (inserted between an electromagnet).

PNR is sensitive to the nuclear and in-plane magnetic composition throughout the depth of the sample (the neutron absorption cross sections for the atomic species in the sample are negligible). The scattering-length densities of the magnetic specimen are given by either the sum or the difference of nuclear (ρ_n) and magnetic (ρ_m) components. The neutron interaction potential is given by $\bar{V} = \frac{2\pi\hbar^2}{m}(\rho_n \pm \rho_m) = \frac{2\pi\hbar^2}{m} N b_n \pm \vec{\sigma}\cdot\vec{B}$, where N is the atomic density, b_n is the coherent nuclear scattering length, m is the mass of neutron, B is the internal magnetic field of specimen, and σ represents the operator associated with the Pauli spin matrices. The scattering length densities (SLDs) of a magnetic specimen are given either by the sum or difference of the nuclear (ρ_n) and magnetic (ρ_m) components. The specular reflectivities in the non-spin-flip channels (R_{++} and R_{--}) yield information about the magnetization component collinear to H_a. Here + and − signs that refer to the intensity R represent the polarization parallel and antiparallel to the guiding field. Fits to the experimental data were done by taking into account the background level and the polarizing and analyzing inefficiencies. We consider several mixed layers of Ge, Fe, and Mn capped with another layer of ZnS. Such a modulation within the DMS layer improves the fits significantly as compared to a constant SLD profile signifying the sensitivity of the present data on the SLD profile.[14]

Specular scattering measures the depth variation in lateral average interaction potential from different coherent volumes. The scattering along the thickness of the specimen can be considered coherent as the perpendicular projection of the neutron coherence length ($l_\perp$) extends over several microns and hence the depth sensitivity. Earlier, a quantitative information on depth profile has been shown for GaMnAs type of specimens.[10] Within the *kinematical* (limited to high Q) treatment of the data, reflectivity is related to the derivative of the density profile ($d\rho/dz$) and the autocorrelation function ($d\zeta/dz$) is given by the Fourier transform of $R(Q) \times Q^4$. Alternatively, exact reflection coefficients can be retrieved within the *dynamical* approach (low Q) following the Parratt formulism.[17] Here a model density profile is considered (prior knowledge of the scattering density), which should be sufficiently close to the correct one. The variation in the magnetization vector (in-plane amplitude and direction) with depth can thus be extracted as the reflection amplitude is related to the Fourier transform of the SLD depth profile. We have followed the dynamical way for our fitting models.

III. EXPERIMENTAL RESULTS

Segregation, upon annealing of a DMS layer, can be identified by a movement of magnetic species along the thickness of the sample. Such segregated magnetic species are susceptible to form small clusters usually at the top of the layer surface often acting as isolated domains within the semiconductor matrix and therefore it cannot be considered as a true DMS layer anymore. A homogeneous layer is characterized by a single magnetic phase (DMS4Fe2Mn) while clustered species can lead to a second phase (DMS2Fe4Mn). Now as our specimens are covered with a cap layer, it is likely that the magnetic species may have even moved into the cap layer of ZnS (altering ρ_m and ρ_n for both layers). Therefore, we employ here two different models for our data fits. Model 1 (M_1) considers no segregation of species (magnetic) onto the top cap layer (here ρ_m for ZnS is restricted to zero while the individual thicknesses and SLD components act as free parameters), while model 2 (M_2) considers a segregation of codopants (here ρ_m for ZnS also act as a free parameter). By comparing these two situations, employing M_1 and M_2, for a single specimen, we should be able to identify any segregation in the sample.

Figure 1 compares the spin asymmetries (SAs) (difference in R_{++} and R_{--} divided by the sum of the two) at 50 K and at saturation measured at TREFF. We consider two different models in fitting the data: (a) the fits, shown as black lines, correspond to the treatment of the data within M_1 and (b) the fits to the data within M_2 (gray lines) have also been drawn. Also provided are the reflectivity patterns with best fits and SLD variation in depth for the respective models. It can be clearly followed, comparing the goodness of fit factor (χ^2) to the respective reflectivity patterns employed with M_1 and M_2. No improvement in χ^2 (worsen by ~ 0.07) is obtained for DMS4Fe2Mn, while for DMS2Fe4Mn a clear improvement (by ~ 0.05) is achieved when M_2 is employed. Therefore, it can be concluded that a sufficient level of segregation of magnetic species into the cap layer has taken place in DMS2Fe4Mn (inhomogeneities for higher Mn-doped specimens). While in DMS4Fe2Mn, no such segregation is indicated by PNR.

Now we look into the field dependence of SA at $Q = 0.017$ Å^{-1} in Fig. 2 from similar measurements at different reflectometers.[14] Both specimens show nonlinear behavior. Interestingly, such nonlinearity can be considered as an indication of clustering,[18] whereas a linear variation indicates noninteracting (para)magnetic species. Further, a difference in their SA behavior, visible over a range of fields, is strongly indicative of different magnetic interactions in two specimens, as we alter the codopant concentration of Mn and Fe. One can easily observe that DMS2Fe4Mn attains saturation much earlier than that by DMS4Fe2Mn. Interaction of clusters is also indicated by the temperature dependence of SA for DMS2Fe4Mn.

For a number of noninteracting superparamagnetic clusters (N_c) with cluster magnetic moment μ_c, the magnetization scales as $M(H,T) = \frac{N_c \mu_c^2 H}{3K_b T}$ (Langevin function $L(x)$ is approximated for small x). The average magnetic moments per magnetic atom (μ_m), estimated from the fitted values of ρ_m,

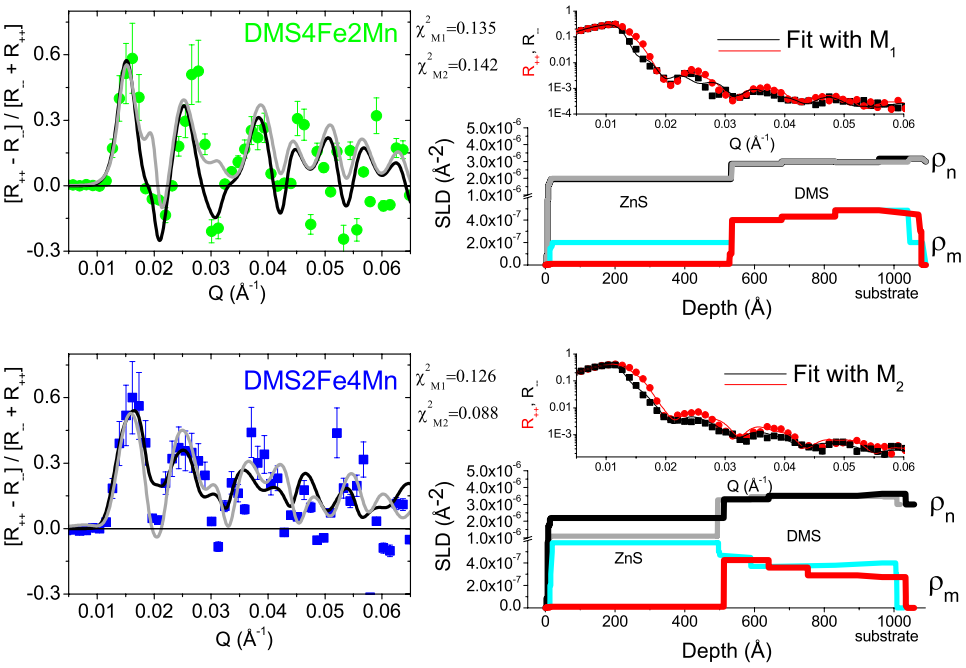

FIG. 1. (Color online) Comparison of the data recast as SA for DMS4Fe2Mn (upper panel) and DMS2Fe4Mn (lower panel) measured at TREFF at a saturation field and at 50 K. The fits within the M_1 (black lines) and M_2 (gray lines) along with the respective SLD variation with depth, plotted in black/red (M_1) and gray/cyan (M_2) lines are shown. The corresponding reflectivity patterns (symbols) and their best fits (lines) are also provided alongside.

are $0.014\mu_B$ (DMS4Fe2Mn) and $0.025\mu_B$ (DMS2Fe4Mn), respectively (here μ_B is the Bohr magneton).[19] Now, considering a number of magnetic atoms to be comprised of one such cluster, the number of clusters is found to be predominantly higher in DMS2Fe4Mn (lower Fe concentration). Such clustering tendencies are well in agreement with the earlier TEM and SQUID measurements as well (insets of Fig. 2).[8,13]

IV. THEORETICAL CALCULATIONS

In order to understand the effect of Fe doping on the chemical and magnetic interactions in MnGe, we have performed first-principles density-functional calculations based on Korringa-Kohn-Rostoker coherent-potential approximation.[20] The Heisenberg interatomic pair-exchange parameters were calculated using the theory of Liechtenstein *et al.*,[21] where the exchange interaction between two spins is calculated using a classical Heisenberg Hamiltonian utilizing the magnetic force theorem. The pair-exchange parameters can be calculated as

$$J_{ij} = \frac{1}{4\pi}\int^{E_F} dE \ \mathrm{Im}\ \mathrm{Tr}_L(\Delta_i T_\uparrow^{ij} \Delta_j T_\downarrow^{ji}), \tag{1}$$

where $\Delta_i = t_{i\uparrow}^{-1} - t_{i\downarrow}^{-1}$, t being the on-site scattering matrix. T is the scattering path operator that is related to the off-diagonal element of Green's function. Tr_L is the trace over the orbital indices of the scattering matrices. Ferromagnetic (antiferromagnetic) interactions are indicated by positive (negative) values of J_{ij}'s. Using the generalized perturbation method,[22] the chemical pair interactions have also been calculated. The effective pair interaction can be written for a sublattice containing a binary alloy AB as

$$V_{ij} = V_{ij}^{AA} - 2V_{ij}^{AB} + V_{ij}^{BB}, \tag{2}$$

where $V_{ij}^{\alpha\beta}$ is the interaction energy when i and j sites are occupied by α and β atoms, respectively.

In the theoretical calculations, the initial alloy composition was taken as $Mn_{19}Ge_{81}$ according to the composition of the multilayer geometry considered in the experiments. Gradually, we varied the Fe concentration by substituting Mn by Fe atoms. For the initial composition without Fe, the magnetic pair-exchange parameter had many antiferromagnetic components those gave rise to a net onsite interaction parameter $J_0^i = \Sigma_n J_{ii}$, which is also antiferromagnetic. The results of Fe doping are shown in Fig. 3. Our calculated onsite exchange parameter J_0 shows that Fe codoping results in ferromagnetic interaction between Fe atoms. Also the antiferromagnetic interaction between Mn atoms in the case of pure Mn-doped Ge becomes weaker on Fe doping. This is in agreement with the experimental observation of an increase in the ordering temperature upon Fe doping.[7,8] In Fig. 4, we

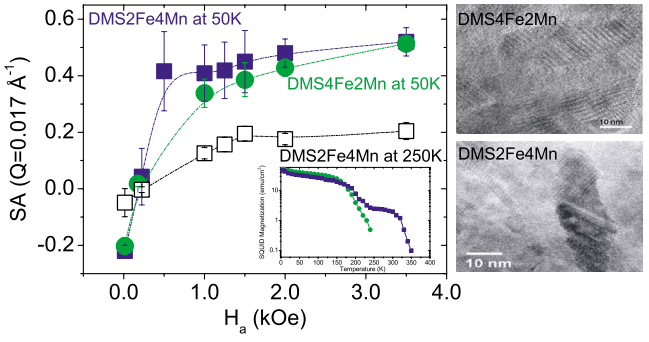

FIG. 2. (Color online) SA for DMS4Fe2Mn and DMS2Fe4Mn from the neutron measurements at reflectometers HADAS/TREFF as a function of applied magnetic field. The lines are guides for the eyes. Corresponding TEM images and SQUID magnetization (logarithmic scale) also indicating the inhomogeneity in DMS2Fe4Mn are reproduced from Ref. 8.

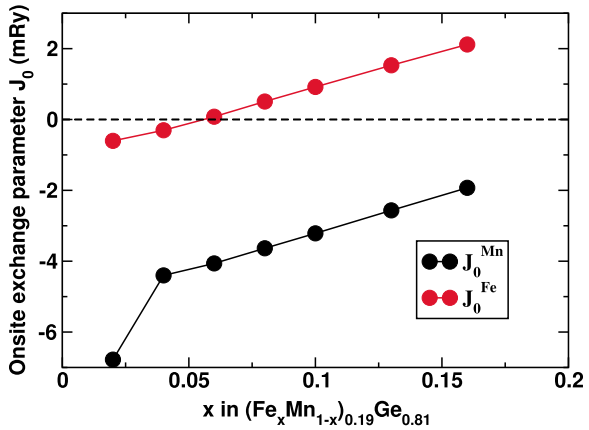

FIG. 3. (Color online) Calculated on-site exchange interaction on Mn and Fe atoms as a function of Fe concentration. A positive (negative) sign indicates ferromagnetic (antiferromagnetic) interactions.

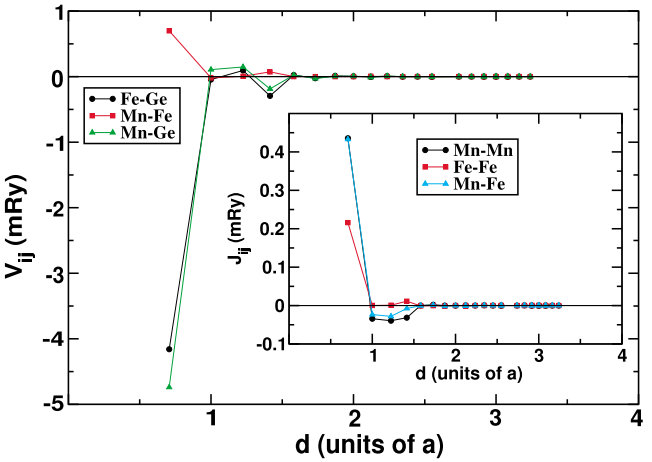

FIG. 4. (Color online) Calculated chemical pair interaction parameters between different species for an alloy composition $Fe_{0.06}Mn_{0.13}Ge_{0.81}$. The corresponding magnetic exchange parameters are shown in the inset.

show the effective chemical pair interaction parameter as a function of distance between a pair of atoms for an alloy composition $Fe_{0.06}Mn_{0.13}Ge_{0.81}$. It should be mentioned that in pure Mn-doped Ge, a strong clustering tendency between the Mn atoms is observed in our calculation. This is a general observation for many diluted magnetic semiconductors.[3,4] In presence of Fe, the effective chemical pair interaction between Mn and Fe is positive signifying a segregating behavior that counteracts the clustering tendency. So, one can expect that the fraction of homogeneity in the codoped system is increased. The resulting magnetic interactions are shown in the inset of Fig. 4 where it is shown that the magnetic coupling between Fe atoms is ferromagnetic unlike between Mn atoms. Also, a careful observation reveals that the exchange interaction between Mn and Fe is less antiferromagnetic than that between Mn atoms. So, an effective increase in the ferromagnetic interaction is possible. All these conclusions are favorable toward making this codoped magnetic semiconductor attractive for applications.

V. CONCLUSION

In conclusion, we have shown the potential of Mn- and Fe-codoped Ge as a candidate for spintronics applications. PNR could not only indicate a difference in inhomogeneities for alternate concentration of Mn and Fe within the Ge matrix, but it also could effectively indicate lower clustering tendencies for higher Fe doping. In agreement with experiments, theoretical calculations reveal that Fe doping in MnGe results in an increase in ferromagnetic interactions as well as a decrease in the overall clustering tendency between the magnetic dopants, the two facts making this system important for applications.

ACKNOWLEDGMENTS

A.P. would like to thank D. E. Bürgler for providing the samples and S. Mattauch for his support at TREFF. The experimental work was mostly done during A.P.'s tenure with Forschungszentrum Juelich, Germany. B.S. acknowledges Swedish Research Council for providing financial support and Swedish National Infrastructure for Computing (SNIC) for granting computational time. I. A. Abrikosov and A. V. Ruban are acknowledged for providing the KKR-ASA code.

*Author to whom correspondence should be addressed; amitesh.paul@helmholtz-berlin.de

[1] H. Ohno, J. Magn. Magn. Mater. **200**, 110 (1999).
[2] Y. D. Park *et al.*, Science **295**, 651 (2002).
[3] S. Kuroda, N. Nishizawa, K. Takita, M. Mitome, Y. Bando, K. Osuch, and T. Dietl, Nature Mater. **6**, 440 (2007).
[4] B. Sanyal, R. Knut, O. Grånäs, D. M. Iusan, O. Karis, and O. Eriksson, J. Appl. Phys. **103**, 07D131 (2008).
[5] H. Munekata, H. Ohno, S. von Molnar, A. Segmuller, L. L. Chang, and L. Esaki, Phys. Rev. Lett. **63**, 1849 (1989).
[6] J.-S. Kang *et al.*, Phys. Rev. Lett. **94**, 147202 (2005).
[7] R. Gareev, Yu. V. Bugoslavsky, R. Schreiber, A. Paul, M. Sperl, and M. Döppe, Appl. Phys. Lett. **88**, 222508 (2006).
[8] H. Braak, R. R. Gareev, D. E. Bürgler, R. Schreiber, P. Grünberg, and C. M. Schneider, J. Magn. Magn. Mater. **286**, 46 (2005); H. Braak, Ph.D. thesis, University of Köln, 2006.
[9] B. A. Collins, Y. S. Chu, L. He, Y. Zhong, and F. Tsui, Phys. Rev. B **77**, 193301 (2008).
[10] B. J. Kirby, J. A. Borchers, J. J. Rhyne, S. G. E. te Velthuis, A. Hoffmann, K. V. O'Donovan, T. Wojtowicz, X. Liu, W. L. Lim, and J. K. Furdyna, Phys. Rev. B **69**, 081307(R) (2004).
[11] H. Kępa, J. Kutner-Pielaszek, A. Twardowski, C. F. Majkrzak, J. Sadowski, T. Story, and T. M. Giebultowicz, Phys. Rev. B **64**, 121302(R) (2001).

[12] P. Gambardella *et al.*, Phys. Rev. B **75**, 125211 (2007).
[13] A. Paul, H. Braak, D. Buergler, R. Screiber, D. Rata, P. Gruenberg, C. Schneider, and T. Brueckel, Physica B **397**, 59 (2007).
[14] A. Paul, T. Charlton, and A. Wildes (unpublished).
[15] TREFF at FRM-2 is the recomissioned instrument HADAS from FRJ-2, http://www.frm2.tum.de/.
[16] A. Paul, M. Buchmeier, D. E. Bürgler, U. Rücker, and C. M. Schneider, Phys. Rev. B **77**, 184409 (2008).
[17] C. F. Majkrzak and N. F. Berk, Physica B **221**, 520 (1996).
[18] J. Swerts, K. Temst, C. Van Haesendonck, H. Fritzsche, V. N. Gladilin, V. M. Fomin, and J. T. Devreese, Europhys. Lett. **68**, 282 (2004).
[19] Assuming atomic density of magnetic species to be $0.19N_{\mathrm{Ge}}$ and using the equation $\rho_m = N\frac{\mu_m}{\mu_B}2.695\times10^{-6}$ nm.
[20] I. A. Abrikosov and H. L. Skriver, Phys. Rev. B **47**, 16532 (1993); A. V. Ruban and H. L. Skriver, Comput. Mater. Sci. **15**, 119 (1999).
[21] A. I. Liechtenstein, M. I. Katsnelson, V. P. Antropov, and V. A. Gubanov, J. Magn. Magn. Mater. **67**, 65 (1987).
[22] F. Ducastelle and F. Gautier, J. Phys. F: Met. Phys. **6**, 2039 (1976).